HHS Public Access

Author manuscript

Biochemistry. Author manuscript; available in PMC 2016 February 19.

Published in final edited form as:

Biochemistry. 2016 February 9; 55(5): 743–750. doi:10.1021/acs.biochem.5b01177.

α,β-Dehydro-Dopa: A Hidden Participant in Mussel Adhesion

Razieh Mirshafian[†], **Wei Wei**[†], **Jacob N. Israelachvili**[‡], and **J. Herbert Waite**[†,§,*]

[†]Marine Science Institute, University of California, Santa Barbara, California 93106, United States

[‡]Department of Chemical Engineering, University of California, Santa Barbara, California 93106, United States

[§]Department of Molecular, Cell & Developmental Biology, University of California, Santa Barbara, California 93106, United States

Abstract

Dopa (L-3,4-dihydroxyphenylalanine) is a key chemical signature of mussel adhesive proteins, but its susceptibility to oxidation has limited mechanistic investigations as well as practical translation to wet adhesion technology. To investigate peptidyl-Dopa oxidation, the highly diverse chemical environment of Dopa in mussel adhesive proteins was simplified to a peptidyl-Dopa analogue, *N*-acetyl-Dopa ethyl ester. On the basis of cyclic voltammetry and UV–vis spectroscopy, the Dopa oxidation product at neutral to alkaline pH was shown to be α,β-dehydro-Dopa (Δ**D**), a vinylcatecholic tautomer of Dopa-quinone. Δ**D** exhibited an adsorption capacity on TiO_2 20-fold higher than that of the Dopa homologue in the quartz crystal microbalance. Cyclic voltammetry confirmed the spontaneity of Δ**D** formation in mussel foot protein 3F at neutral pH that is coupled to a change in protein secondary structure from random coil to β-sheet. A more complete characterization of Δ**D** reactivity adds a significant new perspective to mussel adhesive chemistry and the design of synthetic bioinspired adhesives.

Graphical abstract

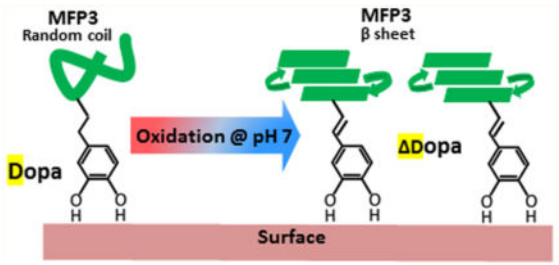

*Corresponding Author: waite@lifesci.ucsb.edu.

Notes

The authors declare no competing financial interest.

Supporting Information

The Supporting Information is available free of charge on the ACS Publications website at DOI: 10.1021/acs.biochem. 5b01177. HPLC results of purified Dopa oxidation products (S_1), mass spectra of **D** (S_2), UV–vis spectrum of synthesized **D** (S_3), plot of current versus the square root of the scan rate (S_4), HPLC results of purified (Δ**D**) (S_5), CV of caffeic acid (S_6), HPLC results of purified polymer and $\Delta\mathbf{QM_B}$ (S_7), CVs of **D** at different pHs (S_8), and FTIR second derivatives (S_9) (PDF)

Mussels are well-known for their ability to adhere to a variety of solid surfaces under saline, fouling, and corrosive conditions.[1–3] At best, synthetic glues, by comparison, are capable of modest or no adhesion under similar conditions.[4] These disparate capabilities have spurred the scrutiny of mussel foot proteins (Mfps), which are rich in the catecholic amino acid known as 3,4-dihydroxy-L-phenylalanine (Dopa). Peptidyl-Dopa residues fulfill at least two essential requirements for practical adhesive bonding: (1) adsorption and (2) cohesion. On mineral surfaces,[5,6] the bidentate H-bonding and coordination chemistry of catechol assures strong adsorption to surfaces. Known cohesive interactions include H-bonding, [7] Fe^{3+} chelation,[8] and covalent cross-linking following oxidation.[9] Little is known about how Dopa is earmarked for one or more of these pathways or how mussels regulate the redox balance of Dopa. *o*-Quinone, a two-electron, two-proton oxidation product of Dopa, is readily detectable at acidic pH;[10] however, in the presence of O_2 at neutral to alkaline pH,[4,11] neither peptidyl-Dopa nor its *o*-quinone is particularly stable.[10]

Both acidic and alkaline pH regimes are relevant to mussel adhesion. Acidic conditions (pH range of ~2–5.5) prevail during the formation of a new adhesive plaque and are imposed under the compliant cuplike mussel foot as it presses against a target surface and secretes Mfp3 and 5.[12] The low pH as well as added thiolate antioxidants (i.e., Mfp6) provides strong reducing conditions for Dopa-containing Mfps and mediates their bidentate adsorption to surface oxides.[10,12] Once the adhesive plaque is fully assembled, the foot retracts, thereby allowing ambient seawater to equilibrate the new plaque[13,14] to pH ~8. Unless protected by coordination to borate or Fe^{3+} or bound to the surface, peptidyl-Dopa is highly susceptible to oxidation at pH 8,[15] and oxidation compromises adsorption. Monolayers of Mfp3 and 5 with intact Dopa exhibit the strongest adhesion to mica when deposited and compressed at pH 2–4.[15] Increasing pH during deposition weakened or abolished adhesion but significantly increased the hydrodynamic protein radii, suggesting an extensive conformational change.[15]

Given its role in melanin formation, the redox chemistry of catecholamines such as Dopa and Dopamine has been intensively investigated[16,17] but has limited relevance to peptidyl-Dopa because in melanins the side chain cyclizes with the quinone to form dihydroxyindole, which, except for N-terminal Dopa, is not possible in proteins.[18,19] *N*-Acetyl-Dopamine[17,20–22] is a better model for studying peptidyl-Dopa oxidation, as is *N*-acetyl-Dopa ethyl ester.[23,24] Both have been studied using UV–vis spectrophotometry with the limitation that many quinone-mediated oxidation products have similar spectra.

Cyclic voltammetry is unquestionably the best technique for exploring the redox properties of peptidyl-Dopa. Cyclic voltammetry (CV) measures oxidation and reduction potentials that reflect structural properties such as the number of conjugated double bonds. An increasing oxidation potential suggests stability against oxidation and can result from more conjugated double bonds. In addition, the peak oxidation current represents the number of transferred electrons and can confirm the presence of catechol functionalities. Furthermore, peak separation gives us some information about electron transfer kinetics.[25]

In this study, we investigated the oxidation chemistry of a low-molecular weight analogue of peptidyl-Dopa, namely *N*-acetyl-Dopa ethyl ester (**D**), by cyclic voltammetry and UV–vis

spectrophotometry. In our previous work,[13] *N*-acetyl-α,β-dehydro-Dopa ethyl ester (Δ**D**) was proposed as an oxidation product of **D**. In this work, we confirmed that oxidation of **D** at neutral to alkaline pH leads to the formation of a quinone tautomer, *N*-acetyl-α,β-dehydro-Dopa ethyl ester (Δ**D**), instead of the expected *N*-acetyl-α,β-Dopa-quinone ethyl ester (**Q**). In contrast to **Q**, Δ**D** retains a catechol moiety, but its adsorption to TiO_2 is 20 times greater than that of Dopa. The unsaturated bond between the side chain and the α-carbon in Δ**D** offers conformational changes not possible in **D**. Δ**D** appears to be relevant to native Mfp3F in that redox properties exhibited by the protein during CV at pH 7 match those of Δ**D**, not those of **D**. Moreover, the conformation of Mfp3F changed from random coil to β-sheet during the oxidation of **D** to Δ**D**. The further oxidation of Δ**D** to an *o*-quinone tautomerizes to dehydro-Dopa-quinone methide B Δ$\mathbf{QM_B}$, which is more resistant to oxidation than **D**. In summary, we show that mussels have a subtle "reserve" of catechol-based adhesive chemistry at pH 7–8. The primary function of this strategy remains to be determined but offers significant new opportunities for surface bonding, metal chelation, covalent cross-linking, and secondary protein conformation.

EXPERIMENTAL PROCEDURES

Enzyme-Catalyzed Synthesis of D

Mushroom tyrosinase (0.1 mg) was added to 1 mg of *N*-acetyltyrosine ethyl ester (**T**) in 10 mL of phosphate-buffered solution (0.1 M PBS) containing sodium borate (0.05 M) at pH 7, and then the solution was mixed gently for 1 h. Glacial acetic acid (1 mL) was added to stop the reaction. The mixture was subjected to reverse phase HPLC using a C18 column (260 mm × 7 mm, Applied Biosciences Inc.) and eluted with a linear gradient (0 to 100% over 40 min) of aqueous acetonitrile. The eluent was monitored continuously at 230 and 280 nm. Two peaks were observed at 22 and 25 min (S_1). The peaks were assessed by TOF mass spectroscopy (S_2). The peak at 22 min corresponds to the 268 Da mass that is consistent with **D**, and the mass of the second peak at 25 min was 252 Da, which is consistent with **T**. Finally, the presence of a sharp λ_{max} at 280 nm in the UV–vis spectrum confirmed the **D** structure (S_3). The yield of synthetic **D** was 80%.

Cyclic Voltammetry

Cyclic voltammetry was performed on a Versastat 3 potentiostat from Ametek Co. These analyses were conducted using a three-electrode cell: a Pt wire as the counter electrode, an Ag/AgCl reference electrode, and a carbon paste electrode (CPE) as the working electrode. CPE is the best choice for adhesive materials because of its ability to be completely polished before each experiment. At pH 4, 0.1 M acetate buffer was used, whereas for pH 7 and 8, PBS was used in the cyclic voltammetry experiments. Catechol autoxidation was avoided by performing all electrochemical experiments with degassed deionized water in a glovebag under argon.

ATR-FTIR Spectroscopy

IR spectra were collected using a Nicolet Magna 850 infrared spectrometer at buffering pH 7, prepared with deuterium oxide (final protein concentration of 1 mg/mL). Data were collected using an attenuated total reflectance (ATR) device equipped with a ZnSe crystal. A

total of 128 scans were taken at a resolution of 4 cm^{-1}. Fourier self-deconvolution was applied to increase spectral resolution in the amide I′ region (1600–1700 cm^{-1}). Origin software (Origin Lab Corp., Northampton, MA) was used to quantify structural components by least-squares curve fitting assuming Gaussian peak shapes with peak centers determined from second-derivative spectra.

QCM Adsorption Experiments

Quartz crystal microbalance (QCM) experiments were conducted with a Q-Sense QCM-D300 instrument to characterize the adsorption of **D** and Δ**D** onto TiO_2 surfaces. The TiO_2 QCM crystals were used as purchased from Q-Sense. Prior to the experiments, the QCM crystals were cleaned in a 2% SDS solution, thoroughly rinsed in the distilled water, dried under nitrogen gas, sonicated for 10 min in ethanol, and then cleaned by UV ozonolysis for 10 min. Frequency and dissipation baselines were established in PBS at pH 7 followed by the injection of 1 mL of a 0.05 mg mL^{-1} solution that began the adsorption experiment.

RESULTS

Cyclic Voltammetry (CV)

A synthetic analogue of peptidyl-Dopa, *N*-acetyl-Dopa ethyl ester or **D**, was prepared in milligram quantities by enzymatic hydroxylation of *N*-acetyltyrosine ethyl ester. **D** was purified for chemical characterization by mass spectrometry and UV–vis spectrophotometry.

CV of 5×10^{-5} M **D** in 0.1 M PBS with a CPE (r = 2 mm) at 0.05 V s^{-1} reveals typical catechols (Figure 1a). **D** undergoes oxidation to **Q** (Scheme 1) with the anodic peak at 310 mV (A_1) corresponding to **D** oxidation, and a reduction peak at 63 mV (B_1) corresponding to **Q** reduction. Both the cathodic and anodic peaks were proportional to the square root of scan rates, $\upsilon^{1/2}$ (S_4), meaning both involved diffusion-limited reactions.[25] Peaks A_2 and B_2 in Figure 1a illustrate the effect of adding periodate to **D** at pH 7 before cyclic voltammetry. Periodate is a strong two-electron oxidant and capable of stoichiometric oxidation of the catechol group. This experiment was performed to investigate whether, upon complete oxidation of **D** to **Q**, further tautomerization of **Q** occurs. Tautomerizations of **Q** to *N*-acetyl-dehydro-Dopa ethyl ester (Δ**D**) or *N*-acetyl-Dopa-quinone methide B ethyl ester are both possible. Δ**D** formation involves the migration of a double bond from the quinone nucleus to the β-carbon in the side chain. The tautomerization of **Q** to Δ**D** needs a Lewis base to extract the acidic proton on the α-^{13}C atom. In our experiments, buffering acetate or phosphate anions could act as Lewis bases to catalyze the rearrangement. Via addition of periodate at a molar ratio of 1:1 (periodate:Dopa), a considerable potential shift toward the negative potential was observed (A_2). The lower oxidation peak at 230 mV (A_2) indicates a new electroactive compound being produced, one more easily oxidized than **D**. Via comparison of the structures of the **D** and Δ**D** oxidation products (Scheme 1), it is evident that dehydro-Dopa-quinone (Δ**Q**) with six conjugated double bonds is more stable than **Q** with four conjugated double bonds. Hence, it seems that the oxidation of Δ**D** is more favorable than that of **D**, and the lower potential of A_2 is largely consistent with this. Further periodate addition (2:1 periodate:Dopa molar ratio) led to detection of another reduction peak at 170 mV (B2) attributed to the formation of Δ**Q** in solution. To confirm Δ**Q**,

oxidation of **D** was independently monitored by UV–vis spectrophotometry. Figure 1b shows the UV–vis spectra of **D** (8×10^{-4} M) upon addition of increasing amounts of periodate. The peak at 280 nm corresponds to the λ_{max} of **D**. Upon addition of periodate, there is a significant absorbance increase at 320 nm characteristic of vinylcatechols, e.g., Δ**D**[13], whereas the λ_{max} at 400 nm, typical of *o*-quinones, rose only modestly. Considering the UV–vis data and the CV results, Δ**D** is clearly the dominant product of **D** oxidation at pH 7. Adding periodate did not decrease the apparent absorbance at 280 nm, because, like other vinylcatechols, Δ**D** has two UV peaks: one at 320 nm due to the conjugation of vinylic and phenolic resonances and the catechol absorbance at 280 nm.

Purification of Oxidation Products

The periodate-induced oxidation and tautomerization reactions of **D** are dependent on time and periodate concentration. Thus, obtaining large quantities of specific oxidation products requires optimization and tuning of reaction conditions. Improved Δ**D** production was attempted using a range of periodate concentrations and resulted in a satisfactory yield (90%) of several specific compounds.

ΔD Purification

In the presence of a 0.1:1 periodate:**D** molar ratio in PBS (pH 7), a peak eluting at 20 min dominated the HPLC chromatogram (C18 column eluted with a linear gradient of aqueous acetonitrile) (S_5). The CV of the first purified compound (Figure 2b) exhibited an oxidation potential peaking at 190 mV (A_2) with reduction occurring at 130 mV (B_2) and a 60 mV peak separation. This signature is distinct from the CV of **D** (Figure 2a) and is more consistent with the Δ**D** CV. The 60 mV peak separation reveals greater reversibility and faster electron transfer kinetics for Δ**D** than for **D**. To further confirm the Δ**D** structure, the CV of caffeic acid, another catechol with a vinylic group in the side chain, was compared with that of Δ**D**. At pH 7, caffeic acid's redox potentials were largely consistent with the Δ**D** CV (S_6).

Purification of ΔQM_B

With an increase in the level of periodate to a molar ratio of 1:1, a 22 min peak appeared in the C_{18} HPLC chromatogram (S_7). CV of this compound exhibited oxidation/reduction peaks at 400 mV (A_3) and −10 mV (B_3), suggesting a stable structure that resists electrochemical change (Figure 2c). Peak separation occurs 410 mV, indicating irreversibility and slow electron transfer kinetics. Moreover, comparing the CV of **D** and the purified 22 min compound at the same concentration reveals that the oxidation peak current of the 22 min compound is only half of that of **D**. The oxidation current depends on the concentration as well as the number of electrons involved in the oxidation process. A peak with half the current at the same concentration suggests a one-electron transfer process instead of the two-electron redox system characteristic of **D**. Considering the one-electron redox chemistry and its high stability, the purified compound is proposed to be dehydro-Dopa-quinone methide B or Δ$\mathbf{QM_B}$, a tautomer of Δ**Q** (Scheme 1). In this experiment, the oxidation current results from oxidation of hydroxyl groups to quinones. Because **D** has two phenolic hydroxyls and Δ$\mathbf{QM_B}$ has just one, a one-electron oxidation is consistent with the

structure of Δ**QM$_B$**. Furthermore, six conjugated double bonds in the structure of Δ**QM$_B$** represent a stable resonance that is difficult to oxidize because of the decrease in the number of conjugated double bonds from six in Δ**QM$_B$** to four in its oxidation product.

Polymerization

Adding excess periodate to **D** resulted in a product eluting at the end of the acetonitrile gradient (100% acetonitrile) (S_7). In contrast with compounds **D** and Δ**D**, this compound (III) was insoluble in both water and ethanol, suggesting a higher hydrophobicity or molecular weight, or both. A polymeric or dimeric structure is likely for the new compound; however, given its insolubility in water, no further characterization was undertaken.

Oxidation Mechanism in Acidic and Alkaline Solutions

To test whether the oxidation products at acidic and alkaline pHs were same as those at pH 7, **D** was exposed to periodate at pH 4 and 8. Figure 3 illustrates the CVs and UV–vis spectra of **D** in acetate buffer (pH 4) and periodate. The most obvious trend in the UV–vis data (Figure 3c) is a decrease in the magnitude of the peak at 280 nm and an increase at 400 nm, indicating **D** consumption and **Q** production. Figure 3a illustrates the CV of **D** at pH 4. Without periodate, **D** ↔ **Q** redox is manifested by peaks at 400 and 200 mV. Given that oxidation of **D** is a two-electron, two-proton transfer reaction, different redox potentials are expected for **D** at different pHs. This trend is confirmed in the Supporting Information (S_8).

Addition of periodate resulted in a drop in peak current at 400 mV (Figure 3a), which was proportional to the absorbance decrease at 280 nm (Figure 3c). However, neither CV nor UV–vis analysis supported the presence of Δ**D** formation during **D** oxidation at acidic pH.

At pH 8, UV–vis spectra and CV of Δ**D** during oxidation by periodate tell a different story (Figure 3b,d). In the UV–vis spectra (Figure 3d), the dominant peak at 320 nm suggests Δ**D** formation. In the CV (Figure 3b), there is no secondary oxidation peak representing Δ**D**, but the second reduction peak at 150 mV can be interpreted as the Δ**D** reduction peak. Perhaps diminution of the quinone peak upon oxidation reflects its tendency to tautomerize. Considering the UV–vis peak at 320 nm and the second reduction peak in CV, Δ**D** formation at pH 8 was confirmed, whereas cyclic voltammetry was not selective enough to resolve overlapping **D** and Δ**D** peaks.

Relevance to Dopa-Containing Proteins: Mfp3F

CV of mussel foot protein Mfp3F was performed at pH 4 and 7, and the results were compared with CV of **D** and Δ**D** with respect to tautomer formation. At pH 4, the similarity between CV of Mfp3F and **D** confirmed the presence of Dopa in Mfp3F (Figure 4). CV of Mfp3F in PBS pH 7 exhibited redox peaks at 200 and 150 mV with a peak separation of 50 mV. Comparison with Δ**D** (Figure 5b) and **D** (Figure 5c) redox reveals that Mfp3F most resembles the Δ**D** redox peaks whereas the **D** redox peaks are separated by 100 mV from the natural protein peak potentials. Hence, we can conclude that at pH 7, the Dopa functionality in Mfp3F had been substantially converted to dehydro-Dopa by the time the CV was taken. A single unsaturated bond in the side chain is the only difference between the Δ**D** and **D** structures but is key to potential conformational changes. Dehydro-Dopa-containing

peptides and proteins have lost the free rotation present in **D** around the α–β carbons.[26] Yu[10] previously showed that Mfp3F monomolecular films have a thicker hardwall in the surface force apparatus (SFA) experiments conducted at pH 7.5 than at pH 3. As the hardwall measured by SFA approximates a protein's hydrodynamic diameter, the pH-dependent increase in the hardwall suggests a conformational change to more ordered secondary structures. The similarity of Δ**D** and Mfp3F CVs at pH 7 revealed formation of a dehydro-Dopa moiety with the unsaturated bond in Mfp3F at high pH. According to the literature,[18,27] unsaturated bonds in the Mfp3F backbone lead to a conformational change from intrinsically unstructured to a β-sheet secondary structure with a corresponding increase in the hydrodynamic radius.[27] Moreover, Mfp3F's conformational change with increasing pH was previously proposed[27] on the basis of circular dichroism experiments. Hence, it can be concluded that the conformational change and increased hardwall are correlated with dehydro-Dopa formation as an oxidation product at high pH. Apparently, dehydro-Dopa can explain both the conformational and dimensional changes of Mfp3F at interfaces.

ATR-FTIR of Mfp3F at pH 7

To investigate the impact of Δ**D** formation on Mfp3F secondary structure, FTIR spectra of Mfp3F were compared at pD 7.4 and 4.4 in deuterated phosphate-buffered saline (Figure 6 and Table 1). The amide I region in ATR-FTIR spectra was used to determine Mfp3f's secondary structure at pH 4 and 7.5. The spectra were deconvoluted according to peak centers determined from second-derivative spectra (Figure S7). The composition of protein conformations under each pH condition was calculated from the area under each deconvoluted peak, which corresponds to specific secondary structures.[28] According to FTIR results, a random coil is the dominant secondary structure of Mfp3F at pH 4 and is consistent with previous circular dichroism analysis of mussel foot proteins.[8] Obviously, the random coil conformation is no longer the dominant secondary structure at high pH. At pH 7, the β-sheet is the dominant secondary structure of Mfp3F. Imazu et al.[27] previously proposed that by helping to form β-turns, dehydrophenylalanine residues stabilized bioactive β-sheets. Given the similarity of dehydrophenylalanine and dehydro-Dopa, the presence of 33% β-sheet structure is consistent with dehydro-Dopa formation in Mfp3F at pH 7.

QCM (adsorption of D and ΔD to TiO_2)

Dopa has emerged as a critical component for protein adhesion, and Dopa-quinone, the product of Dopa oxidation, was shown to greatly reduce the level of adhesion to mineral/metal surfaces. Considering the ease with which Dopa-quinone tautomerizes to Δ**D**, how well dehydro-Dopa containing compounds bind to surfaces becomes an important question. To address this, the adsorption of **D** and Δ**D** on TiO_2 surfaces was compared by QCM (Figure 7). To explore the impact of periodate on adsorption, Δ**D** was presented to TiO_2 with (pre-HPLC) and without periodate (post-HPLC). Figure 7a shows the adsorption of **D** to the TiO_2 sensor surface. As the molecules adsorb, the resonant frequency of the oscillating quartz crystal was damped in proportion to the adsorbed mass on the surface. The QCM also monitors dissipation in the oscillations of the crystal, which increase in proportion to the compliance or viscosity of the adsorbed layer. Typically, small molecules like **D** do not adsorb enough to show much signal change by QCM.[29] The Δf signal, however, is adequate

for **D** and >10-fold greater for Δ**D** (Figure 7a,b), which is extraordinary for such a small molecule. Figure 7c illustrates Δ**D** adsorption with periodate present at ratios of 1:1. Judging by the decrease in frequency, adsorption to TiO_2 is even greater than with purified Δ**D**. Given that periodate-induced Dopa oxidation and associated phenol coupling progress with time, the higher adsorption may be due to oxidation products such as Δ$\mathbf{QM_B}$, dimers, or polymers. As signal saturation occurred in a few minutes for all samples, the QCM sensor was flushed with clean PBS (pH 7) after 10 min. Flushing with buffer essentially returned the frequency and dissipation to initial conditions, indicating that the adsorption of all tested compounds was weak. Using a Voigt model and the viscoelastic equation, the mass and thickness of adsorbed layers are summarized in Table 2.

DISCUSSION

The catecholic Dopa side chains of mussel adhesive proteins (Mfps) are generally regarded as oxidatively unstable functionalities in biochemistry and typically become quinones by a two-electron oxidation. Quinone tautomers are a neglected aspect of mussel adhesive chemistry but are favorably formed from *o*-quinones at pH 7–8 in the oxidative environment of seawater. Given the complexity of Dopa-containing sequences in Mfps, we investigated quinone tautomerization by oxidizing a simple analogue of peptidyl-Dopa **D**, i.e., *N*-acetyl-Dopa ethyl ester. By parallel analysis using CV and UV–vis spectrophotometry, we discovered that Dopa-quinone is not a stable product of peptidyl-Dopa oxidation. Quinone tautomers such as dehydro-Dopa and dehydro-Dopa-quinone methide B are equally or more likely products at pH 7–8 and were hypothesized previously.[13,14] Do these products have a bearing on adhesion? According to QCM results, the level of adsorption of Δ**D** to TiO_2 is 20 times greater than that of **D**. Δ**D** displayed more facile oxidation than **D** because its oxidation peak appeared at lower potentials and, in contrast with **D**, has conformational consequences by recruiting the α-carbon in the peptide backbone into a double bond. More importantly, the redox properties of Mfp3F during CV at pH 7 resemble those of dehydro-Dopa, not Dopa. This finding provides compelling insights for the pH-dependent changes in the hardwall of Mfp3F reported by Yu et al.[10] As the hardwall observed by SFA is a measure of a molecule's hydrodynamic diameter, the different hardwalls at varying pHs have been associated with conformational changes in Mfp3F.[30] Dopa-containing Mfp3F is intrinsically disordered;[8] however, with significant dehydro-Dopa present, another secondary structure is possible due to unsaturated bonds connecting the side chains to the backbone.[30] Autoxidative conversion of Dopa to dehydro-Dopa at pH 7 was confirmed by the similarity of Δ**D** and Mfp3F CV. At an initial acidic pH, Mfp3F has a random coil structure, but as the pH increases and Dopa changes to dehydro-Dopa, Mfp3F undergoes a conformational change to β-sheet, which results in a larger hydrodynamic diameter. This scenario reasonably explains the pH-dependent hardwall.

CV and UV methods also revealed the formation of Δ$\mathbf{QM_B}$ following a second two-electron oxidation and Δ**Q** tautomerization. The higher oxidation potential and just one-electron transfer of Δ$\mathbf{QM_B}$ reveal the mussel's new strategy for coping with the oxidative environment. Under the more oxidative conditions, mussels change their structures to form more conjugated double bonds, thereby arresting further oxidation. Thus, even under very

oxidative conditions, Δ**QM$_B$** formation is favored over **Q** formation. Δ**QM$_B$** is still capable of hydrogen bonding, participating in chelation,[31] and contributing to adhesion. More importantly, it is the most oxidation-resistant molecule in the pathway. The oxidation current of Δ**QM$_B$** is only half that of **D** and Δ**D** at the same concentration, as Δ**QM$_B$** undergoes a one-electron, one-hydrogen transfer reaction whereas **D** and Δ**D** oxidation involves a two-electron, two-hydrogen transfer. The **D** oxidation products were explored in basic and acidic solutions, as well. At pH 8, according the UV–vis data, Δ**D** is the dominant product of **D** oxidation. The decreasing magnitude of the quinone peak and another reduction peak appearing in CV corresponding to Δ**Q** provide additional evidence of making Δ**D** at pH 8 even though CV was not able to distinguish the **D** and Δ**D** oxidation peaks. On the basis of the UV and CV experiments, the Dopa-quinone is the dominant oxidation product of **D** at pH 4.

Results of this study add significant and provocative insights into the biochemistry and technology of mussel-inspired adhesion. The foremost insight is that the oxidative loss of the catecholic moiety of Dopa is recovered in dehydro-Dopa by tautomerization. Although Dopa and dehydro-Dopa remain electrochemically distinct, they are both capable of bidentate H-bonding and metal coordination, and both have reducing power. By QCM, dehydro-Dopa is adsorbed on TiO_2 at a capacity 20 times greater than that of Dopa. Where dehydro-Dopa and Dopa really part ways is in their influence on conformation. The double bond between the α- and β-carbons in dehydro-Dopa locks the side chain into the same plane as the α-amino and α-carboxy groups. Synthetic peptides enriched with dehydro-Phe form stable β-sheets similar to the conformation[30] suggested by SFA studies and confirmed by FTIR in Mfp3F.

CONCLUSION

The catecholic functionality of peptidyl-Dopa can no longer be assumed to disappear upon oxidation of Dopa to Dopa-quinone at pH 7–8. This study reveals that despite formation of transient Dopa-quinone during the two-electron oxidation by periodate, a tautomer known as dehydro-Dopa predominates in solution. Dehydro-Dopa is a catechol with largely unexplored possibilities for both redox and adhesion. Dehydro-Dopa-quinone methide B is the primary stable end product of both Dopa and dehydro-Dopa oxidation and is highly resistant to further oxidation. CV provides convincing support for the presence of dehydro-Dopa in the mussel adhesive protein Mfp3F at pH 7. Formation of high levels of dehydro-Dopa in proteins changed secondary structure due to the formation of unsaturated bonds with backbone carbon atoms. QCM measurements show that dehydro-Dopa has an adsorption capacity 20 times higher than that of Dopa on TiO_2 surfaces. A better understanding of the role of dehydro-Dopa in adhesion will provide the basis for designing tunable synthetic adhesives for underwater and medical applications.

Supplementary Material

Refer to Web version on PubMed Central for supplementary material.

Acknowledgments

Funding

This work was supported by National Institutes of Health Grant R01-DE018468.

We gratefully acknowledge the contribution of Dr. Luigi Petrone from Nanyang Technological University for interpreting FTIR data in this paper.

ABBREVIATIONS

D	*N*-acetyl-Dopa ethyl ester
ΔD	*N*-acetyl-dehydro-Dopa ethyl ester
Q	*N*-acetyl-Dopa-quinone ethyl ester
ΔQ	*N*-acetyl-dehydro-Dopa-quinone ethyl ester
ΔQM_A	*N*-acetyl-dehydro-Dopa-quinone methide A ethyl ester
ΔQM_B	*N*-acetyl-dehydro-Dopa-quinone methide B ethyl ester
HPLC	high-performance liquid chromatography
CV	cyclic voltammetry

References

1. Bandara N, Zeng H, Wu J. Marine mussel adhesion: biochemistry, mechanisms, and biomimetics. J Adhes Sci Technol. 2013; 27:2139–2162.
2. Lee BP, Messersmith PB, Israelachvili JN, Waite JH. Mussel-inspired adhesives and coatings. Annu Rev Mater Res. 2011; 41:99–132. [PubMed: 22058660]
3. Moulay S. Dopa/catechol-tethered polymers: Bioadhesives and biomimetic adhesive materials. Polym Rev. 2014; 54:436–513.
4. Stewart RJ, Ransom TC, Hlady V. Natural underwater adhesives. J Polym Sci, Part B: Polym Phys. 2011; 49:757–771.
5. Yu J, Wei W, Menyo MS, Masic A, Waite JH, Israelachvili JN. Adhesion of mussel foot protein-3 to TiO_2 surfaces: The effect of pH. Biomacromolecules. 2013; 14:1072–1077. [PubMed: 23452271]
6. Lee H, Scherer NF, Messersmith PB. Single-molecule mechanics of mussel adhesion. Proc Natl Acad Sci U S A. 2006; 103:12999–13003. [PubMed: 16920796]
7. Ahn K, Lee DW, Israelachvili JN, Waite JH. Surface-initiated self-healing of polymers in aqueous media. Nat Mater. 2014; 13:867–872. [PubMed: 25064231]
8. Zeng H, Hwang DS, Israelachvili JN, Waite JH. Strong reversible Fe^{3+}-mediated bridging between dopa-containing protein films in water. Proc Natl Acad Sci U S A. 2010; 107:12850–12853. [PubMed: 20615994]
9. Nemes Z, Marekov LN, Steinert PM. Involucrin cross-linking by transglutaminase 1. J Biol Chem. 1999; 274:11013–11021. [PubMed: 10196183]
10. Yu J, Wei W, Danner E, Israelachvili JN, Waite JH. Effects of interfacial redox in mussel adhesive protein films on mica. Adv Mater. 2011; 23:2362–2366. [PubMed: 21520458]
11. Danner EW, Kan Y, Hammer MU, Israelachvili JN, Waite JH. Adhesion of mussel foot protein mefp-5 to mica: An underwater superglue. Biochemistry. 2012; 51:6511–6518. [PubMed: 22873939]
12. Yu J, Wei W, Danner EW, Ashley RK, Israelachvili JN, Waite JH. Mussel protein adhesion depends on interprotein thiol-mediated redox modulation. Nat Chem Biol. 2011; 7:588–590. [PubMed: 21804534]

13. Rzepecki LM, Nagafuchi T, Waite JH. α,β-Dehydro-3,4-dihydroxyphenylalanine derivatives: Potential sclerotization intermediates in natural composite materials. Arch Biochem Biophys. 1991; 285:17–26. [PubMed: 1846730]
14. Rzepecki LM, Waite JH. α,β-Dehydro-3,4-dihydroxyphenylalanine derivatives: Rate and mechanism of formation. Arch Biochem Biophys. 1991; 285:27–36. [PubMed: 1899328]
15. Kan Y, Danner EW, Israelachvili JN, Chen Y, Waite JH. Boronate complex formation with Dopa containing mussel adhesive protein retards pH-induced oxidation and enables adhesion to mica. PLoS One. 2014; 9(10):e108869. [PubMed: 25303409]
16. Ramagopal UA, Ramakumar S, Mathur P, Joshi R, Chauhan VS. Dehydrophenylalanine zippers: strong helix– helix clamping through a network of weak interactions. Protein Eng, Des Sel. 2002; 15:331–335.
17. Sugumaran M, Duggaraju P, Jayachandran E, Kirk KL. Formation of a new quinone methide intermediate during the oxidative transformation of 3,4-dihydroxyphenylacetic acids: implication for eumelanin biosynthesis. Arch Biochem Biophys. 1999; 371:98–106. [PubMed: 10525294]
18. Janes SM, Mu D, Wemmer D, Smith AJ, Kaur S, Maltby D, Burlingame AL, Klinman JP. A new redox cofactor in eukaryotic enzymes: 6-hydroxydopa at the active site of bovine serum amine oxidase. Science. 1990; 248:981–987. [PubMed: 2111581]
19. Grotzinger E, Campbell IM. Intermediate symmetry in lawsone biosynthesis. Phytochemistry. 1972; 11:675–679.
20. Sugumaran M, Semensi V, Kalyanaraman B, Bruce JM, Land EJJ. Evidence for the formation of a quinone methide during the oxidation of the insect cuticular sclerotizing precursor 1,2-dehydro-N-acetyldopamine. J Biol Chem. 1992; 267:10355–10361. [PubMed: 1316899]
21. Paez JI, Ustahüseyin O, Serrano C, Ton X, Shafiq Z, Auernhammer GK, d'Ischia M, del Campo A. Gauging and tuning cross-linking kinetics of catechol-PEG adhesives via catecholamine functionalization. Biomacromolecules. 2015; 16:3811–3818. [PubMed: 26583428]
22. Abebe A, Kuang QF, Evans JJ, Sugumaran M. Mass spectrometric studies shed light on unusual oxidative transformations of 1,2-dehydro-N-acetyldopa. Rapid Commun Mass Spectrom. 2013; 27:1785–1793. [PubMed: 23821572]
23. Sugumaran M, Ricketts D. Model sclerotization studies. 3. Cuticular enzyme catalyzed oxidation of peptidyl model tyrosine and dopa derivatives. Arch Insect Biochem Physiol. 1995; 28:17–32. [PubMed: 7803812]
24. Sugumaran M, Giglio L, Kundzicz H, Saul S, Semensi V. Studies on the enzymes involved in puparial cuticle sclerotization in Drosophila melanogaster. Arch Insect Biochem Physiol. 1992; 19:271–283. [PubMed: 1600191]
25. Bard, AJ.; Faulkner, LR. Electrochemical methods: Fundamentals and applications. 2. Vol. Chapter 6. Wiley; New York: 2001.
26. Ewing AG, Bigelow JC, Wightman RM. Direct in vivo monitoring of dopamine released from two striatal compartments in the rat. Science. 1983; 221:169–171. [PubMed: 6857277]
27. Imazu S, Shimohigashi Y, Kodama H, Sakaguchi K, Waki M, Kato T, Izumiya N. Conformationally stabilized gramicidin S analog containing dehydrophenylalanine in place of D-phenylalanine. Int J Pept Protein Res. 1988; 32:298–30.
28. Susi H, Byler DM. Resolution-enhanced Fourier transform infrared spectroscopy of enzymes. Methods Enzymol. 1986; 130:290–311. [PubMed: 3773736]
29. Zheng B, Cheng S, Liu W, Lam MH-W, Liang H. Small organic molecules detection based on aptamer-modified gold nanoparticles-enhanced quartz crystal microbalance with dissipation biosensor. Anal Biochem. 2013; 438:144–149. [PubMed: 23583908]
30. Wei W, Yu J, Broomell C, Israelachvili JN, Waite JH. Hydrophobic enhancement of Dopa-mediated adhesion in a mussel foot protein. J Am Chem Soc. 2013; 135:377–383. [PubMed: 23214725]
31. Ashkenazi N, Vigalok A, Parthiban S, Ben-David Y, Shimon LJW, Martin JML, Milstein DJ. Discovery of the first metallaquinone. J Am Chem Soc. 2000; 122:8797–8798.

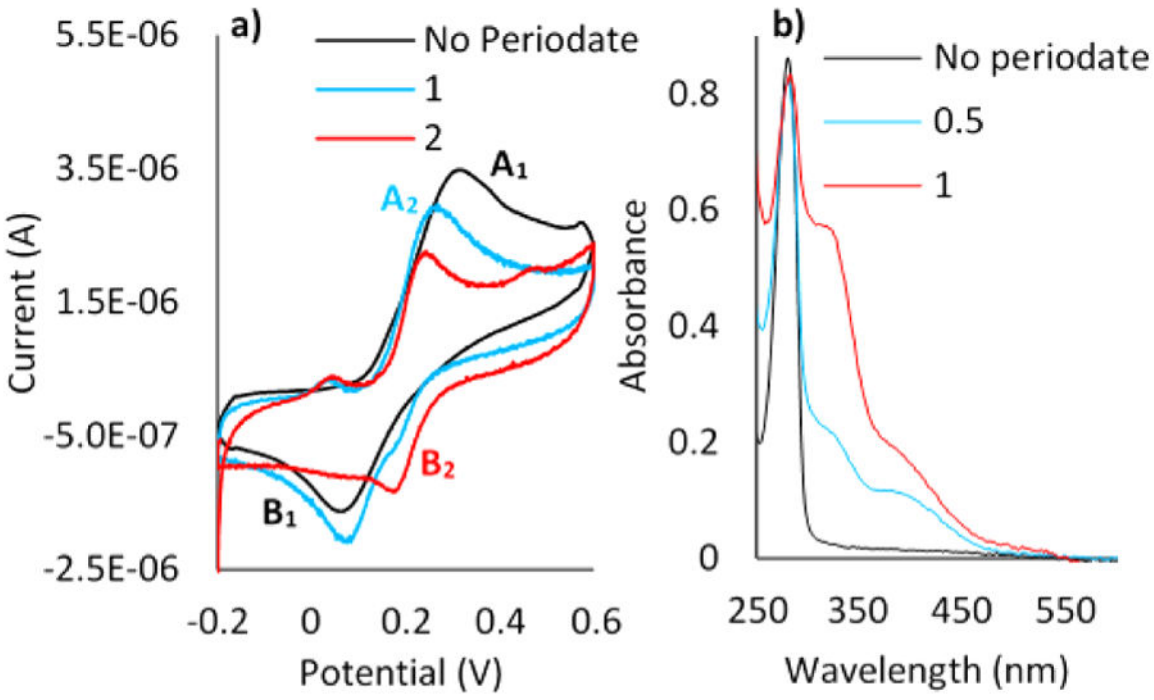

Figure 1.

(a) CV of the CPE electrode in 5×10^{-5} M **D** in 0.1 M PBS (pH 7), with a scan rate of 0.05 V s^{-1}. (b) UV–vis spectra for oxidation of 8×10^{-4} M **D** in 0.1 M PBS (pH 7). The blue curve in panel a) denotes a 1:1 periodate:Dopa ratio, whereas the red curve denotes a 2:1 ratio. In panel b), the blue and red curves denote 0.5:1 and 1:1 periodate: Dopa ratios, respectively.

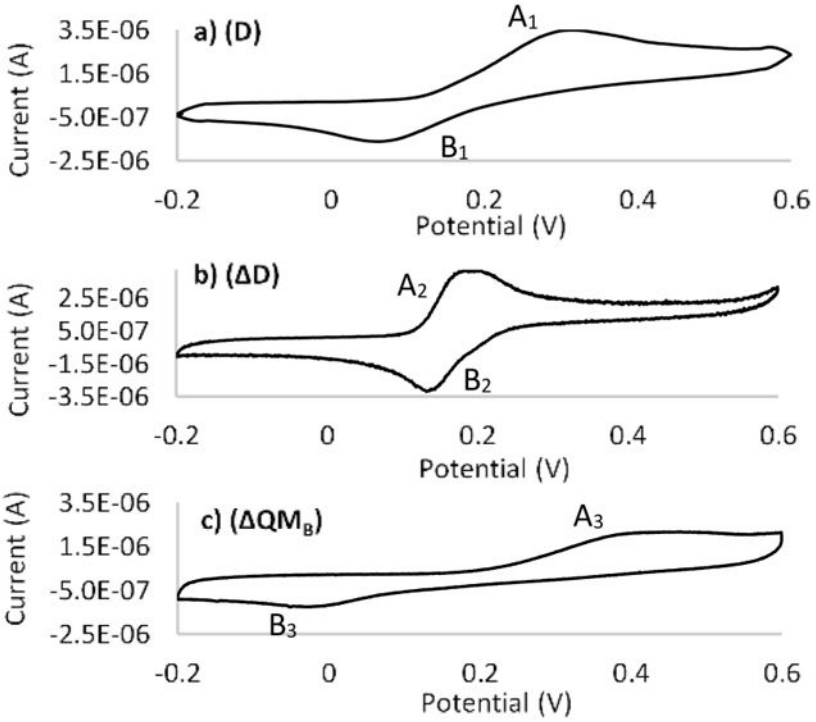

Figure 2.

CVs of (a) purified **D**, (b) Δ**D**, and (c) Δ$\mathbf{QM_B}$ in 0.1 M PBS (pH 7), with a scan rate of 0.05 V s^{-1}.

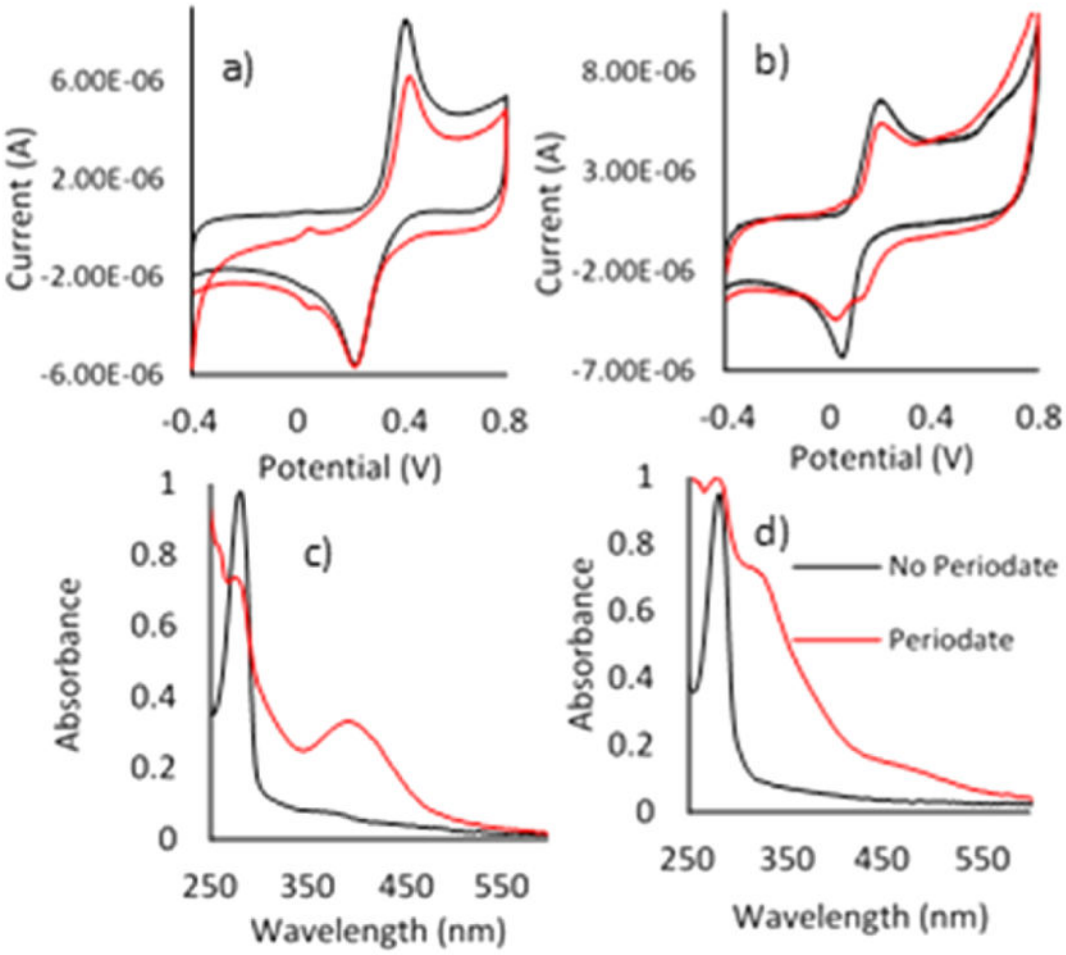

Figure 3.

CV of the CPE electrode in **D** (5×10^{-5} M) (a) in acetate buffer (pH 4) and (b) in 0.1 M PBS (pH 8). UV–vis spectra for oxidation of **D** (8×10^{-4} M) (c) in acetate buffer (pH 4) and (d) in 0.1 M PBS (pH 8), with a scan rate of 0.5 V s^{-1}.

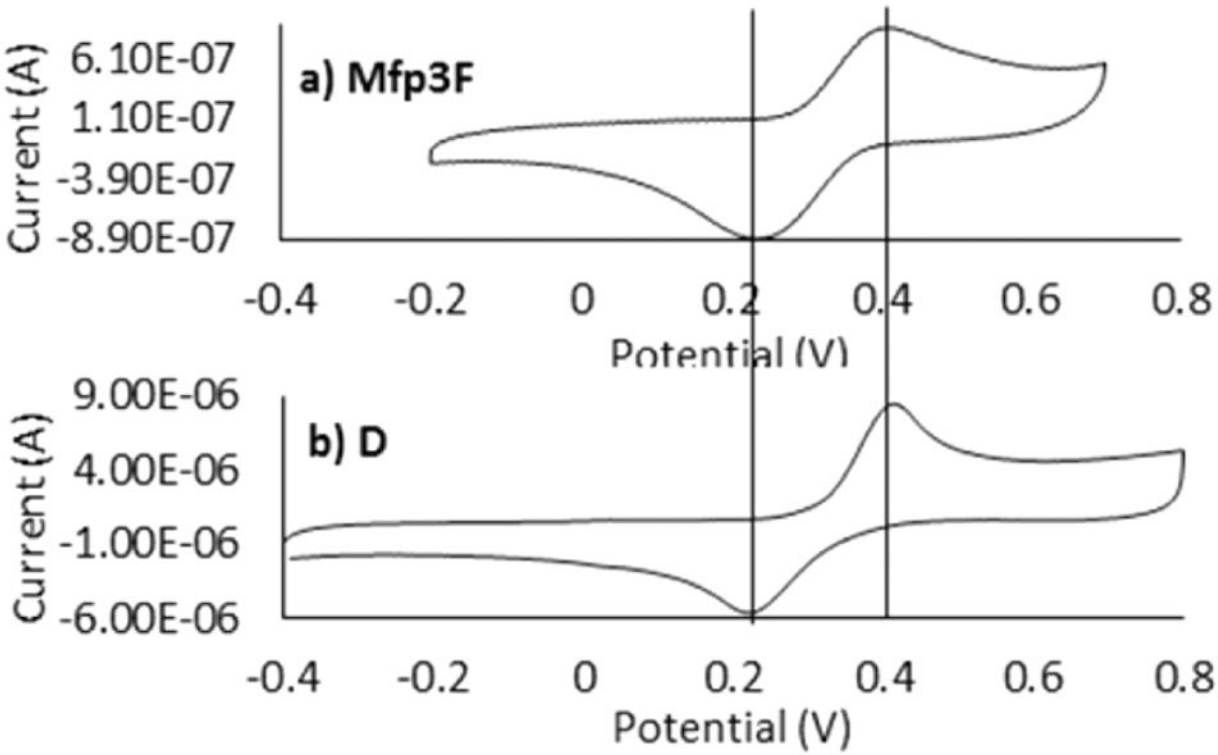

Figure 4.

CVs of (a) Mfp3F and (b) **D** in 0.1 M acetate buffer (pH 4), with a scan rate of 0.05 V s^{-1}.

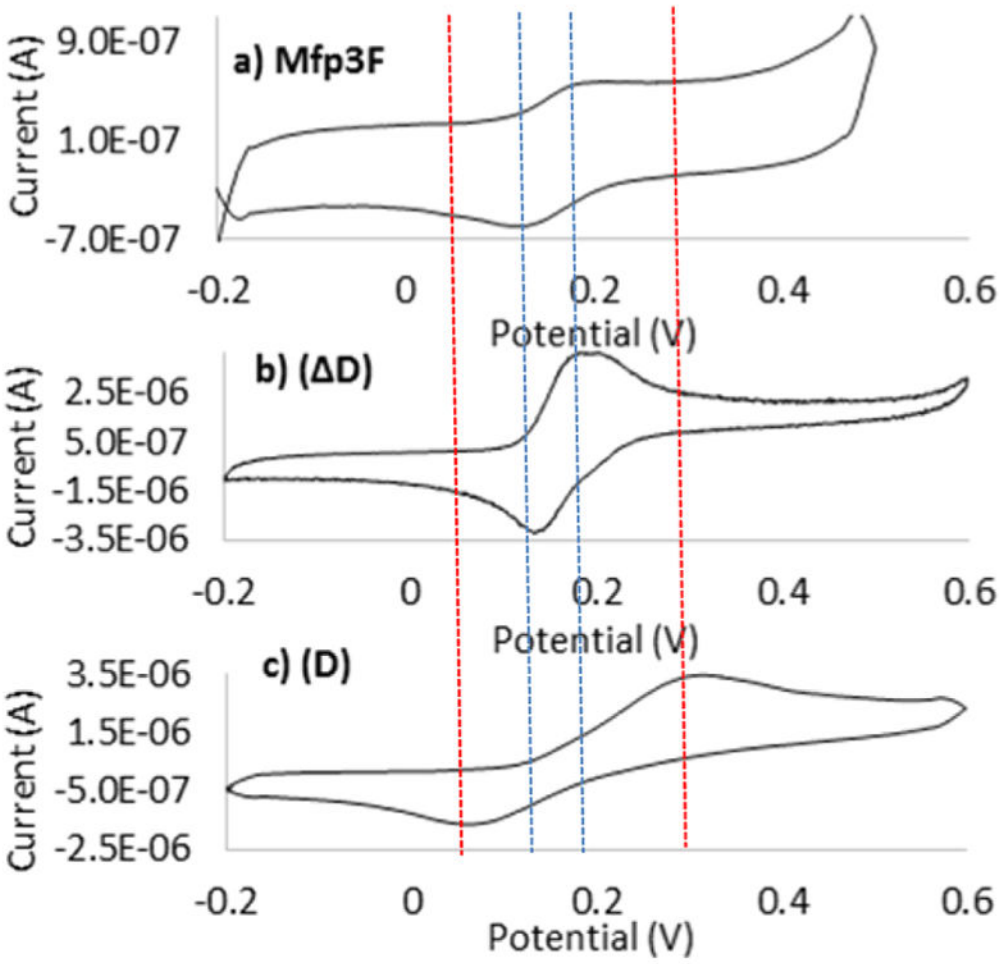

Figure 5.

CVs of (a) Mfp3F, (b) purified Δ**D**, and (c) **D** in 0.1 M PBS (pH 7), with a scan rate of 0.05 V s^{-1}.

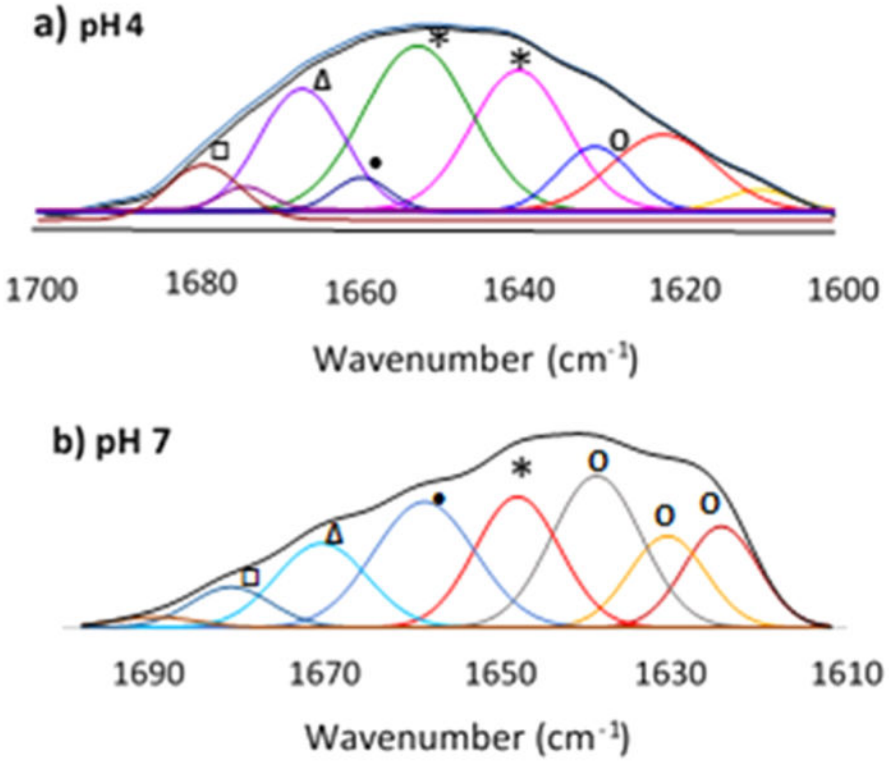

Figure 6.

ATR-FTIR spectra of 1 mg/mL Mfp3F in deuterated buffer at (a) pH 4 and (b) pH 7: (○) *β*-sheet, (*) random coil, (●) *α*-helix, (Δ) 3_{10} helix, and (□) turns. Secondary derivatives are shown in the Supporting Information (S_9).

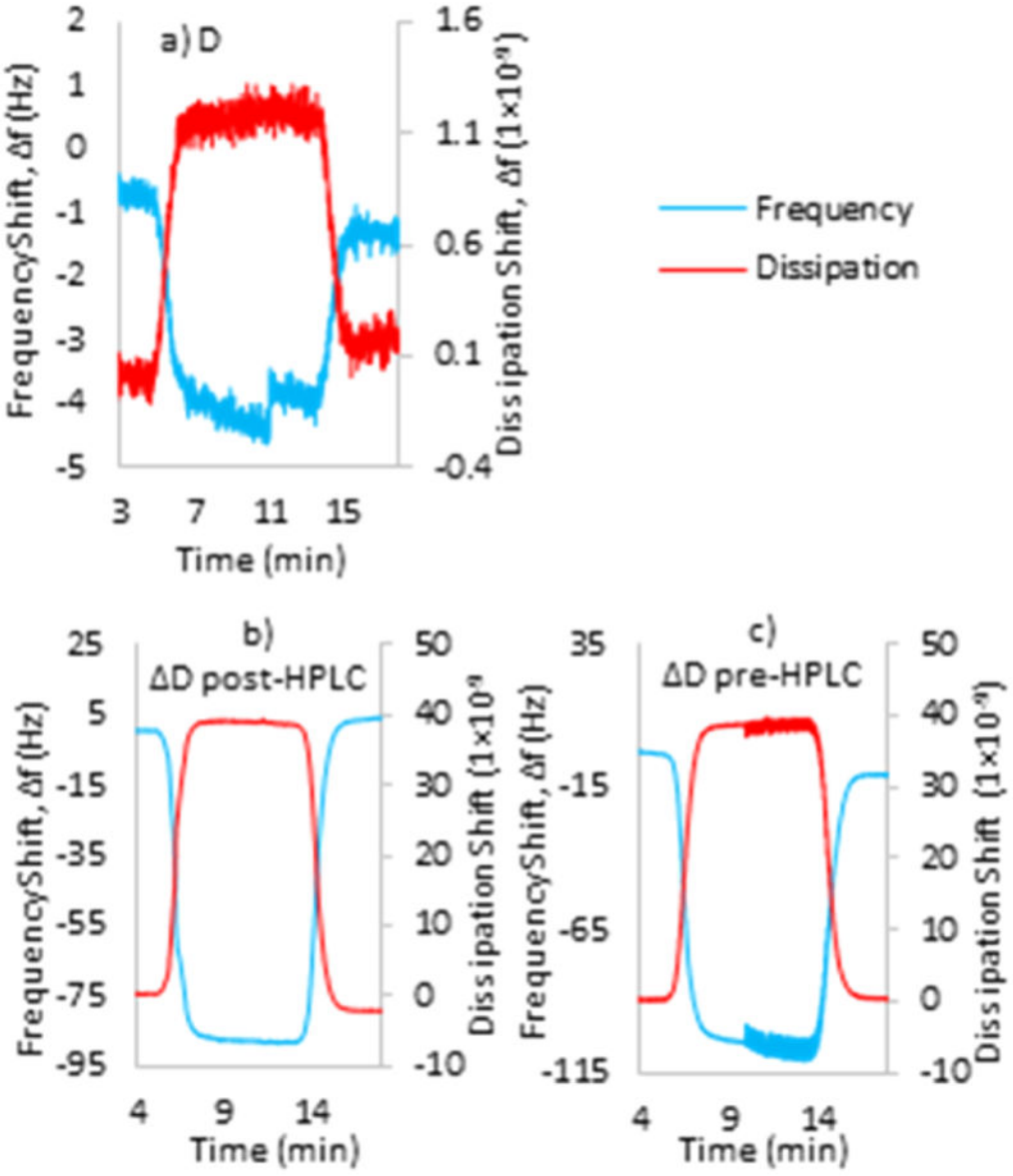

Figure 7.

QCM data of 1 mL of a 0.05 mg mL^{-1} solution of (a) **D**, (b) Δ**D** after HPLC, and (c) Δ**D** before HPLC in 0.1 M PBS (pH 7) on a TiO_2 sensor.

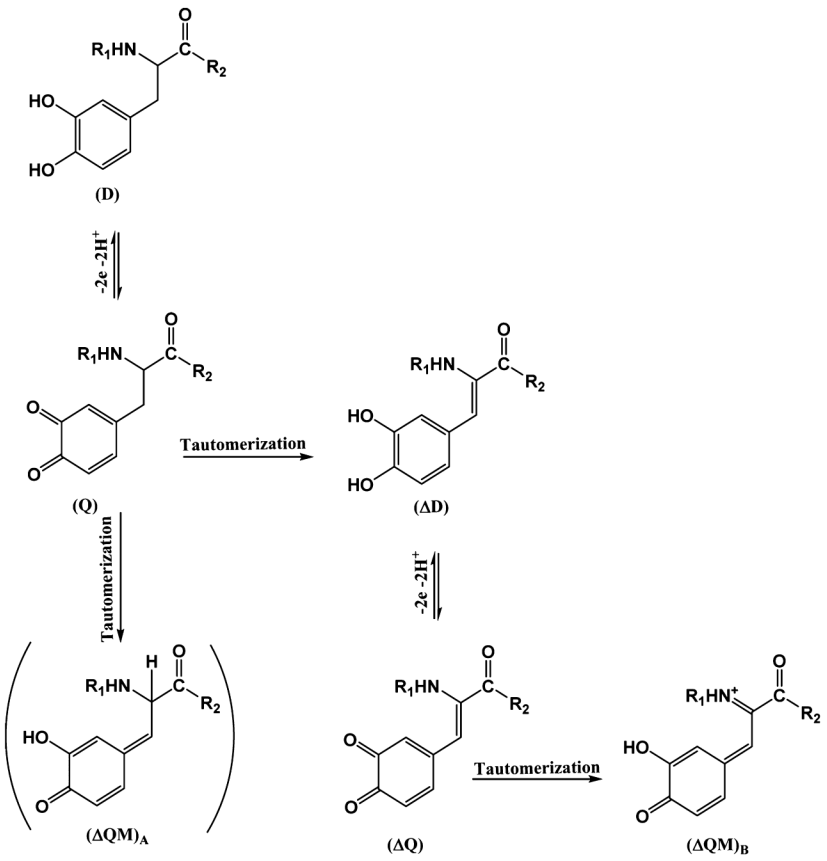

Scheme 1.
Oxidation Mechanism of D at pH 7

Table 1

ATR-FTIR Results and Secondary Structure Compositions of Mfp3F at pH 4 and 7

	secondary structure content (%)	
structure	**pH 4**	**pH 7**
β-sheet	9.5	33
random coil	64	13
α-helix	4	13
3_{10} helix and turns	22	24

Table 2

QCM Data Deduced from the Voigt Model for 1 mL of 0.05 mg mL^{-1} PBS Solutions (pH 7) (±standard deviation; $n = 3$)

sample	thickness (nm)	mass ($\mu g\ cm^{-2}$)
D	0.60 ± 0.05	0.065 ± 0.01
Δ**D** post-HPLC	12 ± 1.6	1.3 ± 0.11
Δ**D** pre-HPLC	430 ± 10	2.5 ± 0.35